CHEMISTRY
A EUROPEAN JOURNAL

DOI: 10.1002/chem.200601354

# Rare-Earth Tricyanomelaminates $[NH_4]Ln[HC_6N_9]_2[H_2O]_7{\cdot}H_2O$ (Ln = La, Ce, Pr, Nd, Sm, Eu, Gd, Tb, Dy): Structural Investigation, Solid-State NMR Spectroscopy, and Photoluminescence

**Abanti Nag,[a] Bettina V. Lotsch,[a] Jörn Schmedt auf der Günne,[a] Oliver Oeckler,[a] Peter J. Schmidt,[b] and Wolfgang Schnick*[a]**

**Abstract:** The rare-earth tricyanomelaminates, $[NH_4]Ln[HC_6N_9]_2[H_2O]_7{\cdot}H_2O$ (LnTCM; Ln = La, Ce, Pr, Nd, Sm, Eu, Gd, Tb, Dy), have been synthesized through ion-exchange reactions. They have been characterized by powder as well as single-crystal X-ray diffraction analysis, vibrational spectroscopy, and solid-state $^{1}H$, $^{13}C$, and $^{15}N$ MAS NMR spectroscopy. The X-ray powder pattern common to all nine rare-earth tricyanomelaminates LnTCM (Ln = La, Ce, Pr, Nd, Sm, Eu, Gd, Tb, Dy) indicates that they are isostructural. The single-crystal X-ray diffraction pattern of LnTCM is indicative of non-merohedral twinning. The crystals are triclinic and separation of the twin domains as well as refinement of the structure were successfully carried out in the space group $P\bar{1}$ for LaTCM (LaTCM; $P\bar{1}$, $Z=2$, $a=7.1014(14)$, $b=13.194(3)$, $c=13.803(3)$ Å, $\alpha=90.11(3)$, $\beta=77.85(3)$, $\gamma=87.23(3)°$, $V=1262.8(4)$ Å$^3$). In the crystal structure, each $Ln^{3+}$ is surrounded by two nitrogen atoms from two crystallographically independent tricyanomelaminate moieties and seven oxygen atoms from crystal water molecules. The positions of all of the hydrogen atoms of the ammonium ions and water molecules could not be located from difference Fourier syntheses. The presence of $[NH_4]^+$ ions as well as two NH groups belonging to two crystallographically independent monoprotonated tricyanomelaminate moieties has only been confirmed by subjecting LaTCM to solid-state $^{1}H$, $^{13}C$, and $^{15}N\{^{1}H\}$ cross-polarization (CP) MAS NMR and advanced CP experiments such as cross-polarization combined with polarization inversion (CPPI). The $^{1}H$ 2D double-quantum single-quantum homonuclear correlation (DQ SQ) spectrum and the $^{15}N\{^{1}H\}$ 2D CP heteronuclear-correlation (HETCOR) spectrum have revealed the hydrogen-bonded (N–H···N) dimer of monoprotonated tricyanomelaminate moieties as well as H-bonding through $[NH_4]^+$ ions and $H_2O$ molecules. The structures of the other eight rare-earth tricyanomelaminates (LnTCM; Ln = Ce, Pr, Nd, Sm, Eu, Gd, Tb, Dy) have been refined from X-ray powder diffraction data by the Rietveld method. Photoluminescence studies of $[NH_4]Eu[HC_6N_9]_2[H_2O]_7{\cdot}H_2O$ have revealed orange-red ($\lambda_{max}=615$ nm) emission due to the $^{5}D_0$–$^{7}F_2$ transition, whereas $[NH_4]Tb[HC_6N_9]_2[H_2O]_7{\cdot}H_2O$ has been found to show green emission with a maximum at 545 nm arising from the $^{5}D_4$–$^{7}F_5$ transition. DTA/TG studies of $[NH_4]Ln[HC_6N_9]_2[H_2O]_7{\cdot}H_2O$ have indicated several phase transitions associated with dehydration of the compounds above 150 °C and decomposition above 200 °C.

**Keywords:** lanthanides · NMR spectroscopy · photoluminescence · structure elucidation · tricyanomelaminates

## Introduction

In recent years, the increased significance of carbon nitride chemistry has been largely attributable to the expected outstanding material properties of binary $C_3N_4$.[1–10] An important building block for binary $C_3N_4$ is the *s*-triazine (cyanuric) ring system "$C_3N_3$", which is linked through trigonal nitrogen atoms forming extended two-dimensional (2D) sheets. Amongst the most familiar precursors for the synthesis of graphitic carbon nitride containing an *s*-triazine ring

[a] Dr. A. Nag, Dr. B. V. Lotsch, Dr. J. Schmedt auf der Günne, Dr. O. Oeckler, Prof. Dr. W. Schnick
Department Chemie und Biochemie, Ludwig-Maximilians-Universität München
Butenandtstrasse 5–13 (D), 81377 München (Germany)
Fax: (+49) 89-2180-77440
E-mail: wolfgang.schnick@uni-muenchen.de

[b] Dr. P. J. Schmidt
Solid-State Lighting, Philips Research Laboratories
Weisshausstrasse 2, 52066 Aachen (Germany)

Supporting information for this article is available on the WWW under http://www.chemeurj.org/ or from the author.

system are melamine (triamino-*s*-triazine) $C_3N_3(NH_2)_3$,[11] cyanuric chloride $C_3N_3Cl_3$,[12–16] and cyanuric azide $C_3N_3(N_3)_3$.[2,6,12,17,18]

The rapidly growing interest in the synthesis of binary $C_3N_4$ has also led to several investigations of ternary C/N compounds, which show promise for applications in coordination and materials chemistry owing to their interesting chemical (e.g., high thermal and chemical stability) as well as optical or magnetic properties.[19–25]

For a long time, the investigation of simple inorganic C/N compounds has been predominantly focused on cyanides. In the past few years, however, other simple C/N compounds containing linear $[N{=}C{=}N]^{2-}$ (carbodiimide) or bent $[N(CN)_2]^-$ (dicyanamide) ions have been recognized as nitridocarbonates, and a number of alkali, alkaline-earth, transition-metal, and rare-earth cyanamides and dicyanamides have been synthesized and characterized in detail.[26–46] Thermolysis of the dicyanamides initiates oligomerization and polymerization processes, leading to extended C/N species. For example, thermolysis of $M^{II}[N(CN)_2]_2$ (M = Mg, Ca, Sr, Ba, Pb)[38,47] or $Ln^{III}[N(CN)_2]_3$ (Ln = La, Ce, Pr, Sm, Nd, Eu, Gd, Tb)[44,46] leads to amorphous products containing undefined polymeric C/N networks, whereas thermolysis of alkali metal dicyanamides $M^I[N(CN)_2]$ (M = Na, K, Rb) results in trimerization of the $[N(CN)_2]^-$ ions with subsequent formation of cyclic tricyanomelaminate ions $[C_6N_9]^{3-}$ (Scheme 1).[35,37,48]

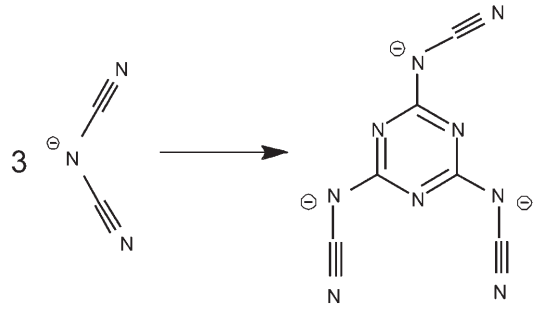

Scheme 1. Trimerization of dicyanamides ($[N(CN)_2]^-$) to form tricyanomelaminates ($[C_6N_9]^{3-}$).

The tricyanomelaminates are built up from a planar *s*-triazine ring system with three N–C≡N cyanamide side arms connected to the carbon atoms of the ring. The respective salts $[M^I]_3[C_6N_9]$ can also be viewed as nitridocarbonates(IV). The crystal structures of both the anhydrous alkali metal tricyanomelaminates (M = Na, K, Rb) and the respective hydrates $Na_3[C_6N_9]\cdot 3H_2O$ and $[M^I]_3[C_6N_9]\cdot H_2O$ (M = K, Rb) have been thoroughly characterized.[35,37,49] Unlike dicyanamides, tricyanomelaminate ($[C_6N_9]^{3-}$) ions undergo acid-base reactions when dissolved in water, forming monoprotonated ($[HC_6N_9]^{2-}$) and diprotonated ($[H_2C_6N_9]^-$) ions with decreasing pH of the solution [Eq. (1)].

$$[C_6N_9]^{3-} + [H_3O]^+ \rightleftharpoons [HC_6N_9]^{2-} + H_2O \quad (1a)$$

$$[HC_6N_9]^{2-} + [H_3O]^+ \rightleftharpoons [H_2C_6N_9]^- + H_2O \quad (1b)$$

To understand these acid–base reactions, detailed knowledge of the syntheses and properties of the mono- and diprotonated tricyanomelaminates is of considerable interest. Only a few protonated tricyanomelaminates have been described in the literature. The monoprotonated tricyanomelaminates $M^{II}[HC_6N_9]\cdot 3H_2O$ (M = Co, Ni, Cu, Cd)[50] and the diprotonated $Co[H_2C_6N_9]_2[H_2O]_4\cdot 6H_2O$[51] were synthesized by acidifying solutions of the corresponding non-protonated tricyanomelaminate salts. Very recently, $Rb[H_2C_6N_9]\cdot 0.5H_2O$ has been synthesized from an acidic solution of $Rb_3[C_6N_9]\cdot H_2O$.[52] Nonmetal monoprotonated tricyanomelaminate salts with ammonium ($[NH_4]_2[HC_6N_9]$) or melaminium cations ($[C_3N_6H_7]_2[HC_6N_9]\cdot 2.4H_2O$) have also been synthesized.[10] Surprisingly, only very few rare-earth compounds containing Ln···N≡C–N units have hitherto been reported, and to the best of our knowledge no tricyanomelaminate salts of trivalent metal ions have been reported to date.

On the other hand, recent investigations concerning rare-earth-doped nitrides (nitridosilicates and oxonitridosilicates) have gained considerable importance in materials science because of the promising applications of these materials as phosphor-converted LEDs.[53] Rare-earth dicyanamides also show interesting photoluminescence properties.[54] This has encouraged us to investigate other rare-earth carbon–nitride compounds with the aim of obtaining better materials for future applications.

Herein, we report the synthesis and structural elucidation of lanthanide tricyanomelaminates $[NH_4]Ln[HC_6N_9]_2[H_2O]_7\cdot H_2O$ (LnTCM) with Ln = La, Ce, Pr, Nd, Sm, Eu, Gd, Tb, and Dy. The crystal structure common to these compounds has been elucidated by a complementary approach based on single-crystal X-ray diffraction analysis accompanied by twin refinement, coupled with a solid-state MAS NMR study on the diamagnetic lanthanum tricyanomelaminate. The latter was instrumental in differentiating between water and ammonium species. The crystal structures of the other eight lanthanide tricyanomelaminates (LnTCM; Ln = Ce, Pr, Nd, Sm, Eu, Gd, Tb, Dy) have been refined from X-ray powder diffraction data using the Rietveld method. Finally, the photoluminescence properties have been examined for $[NH_4]Eu[HC_6N_9]_2[H_2O]_7\cdot H_2O$ and $[NH_4]Tb[HC_6N_9]_2[H_2O]_7\cdot H_2O$.

## Results

**Synthesis and X-ray diffraction analysis of lanthanide tricyanomelaminates**: The synthesis of lanthanide tricyanomelaminates (LnTCM) was initially attempted by using sodium tricyanomelaminate as the starting material. However, the reaction failed due to the high alkaline pH of sodium tricyanomelaminate, which led to the precipitation of lanthanide hydroxides. Therefore, the reaction was carried out using

  

ammonium tricyanomelaminate, whereupon tiny rod-shaped crystals of lanthanide tricyanomelaminates were obtained. The formation of lanthanide tricyanomelaminates was confirmed by spectroscopic studies. The X-ray powder diffraction patterns were indicative of the isostructural nature of all nine lanthanide tricyanomelaminates, LnTCM (Ln = La, Ce, Pr, Nd, Sm, Eu, Gd, Tb, Dy). However, the true compositions of the LnTCM products could not be unambiguously derived from the single-crystal X-ray diffraction studies alone. Close inspection of the single-crystal diffraction pattern of LaTCM reveals split reflections along [010], indicating non-merohedral twinning. Such twinning was found for all of the lanthanide tricyanomelaminates and thus seems to be intrinsic. An attempt was made to solve the crystal structure of lanthanum tricyanomelaminate (LaTCM) from single-crystal X-ray diffraction data. The structure was initially solved by direct methods, neglecting the twinning. During the refinement, the twinning was taken into account through a twin law (1 0 0, 0.182 −1 0, 0.826 0 −1). The crystals were found to be triclinic, with $a = 7.1014(14)$, $b = 13.194(3)$, $c = 13.803(3)$ Å, $\alpha = 90.11(3)$, $\beta = 77.85(3)$, $\gamma = 87.23(3)°$. Separation of the twin domains and refinement of the structure were successfully carried out in the space group $P\bar{1}$. The crystal structure revealed the formula unit of two tricyanomelaminate moieties coordinated to one $La^{3+}$ ion as well as the presence of water molecules. However, the positions of all of the hydrogen atoms could not be determined from difference Fourier syntheses. To establish the exact composition of LnTCM, more detailed investigations were undertaken using solid-state MAS NMR studies in combination with single-crystal X-ray diffraction analysis and infrared spectroscopy.

**Vibrational spectroscopy**: Each of the nine lanthanide tricyanomelaminates (LnTCM; Ln = La, Ce, Pr, Nd, Sm, Eu, Gd, Tb, Dy) was characterized by infrared spectroscopy. The IR spectra of these LnTCM compounds were found to be broadly similar to those of other reported tricyanomelaminates.[47,48,52] The presence of tricyanomelaminate ions in the LnTCM compounds could be easily inferred from their IR spectra by comparison with that of the known compound sodium tricyanomelaminate (Figure 1). The sharp absorption at 2200 $cm^{-1}$ and the bands around 575 $cm^{-1}$ can be assigned to the C≡N stretching vibration and out-of-plane deformation γ(N−C≡N) modes of the cyanamide side arms of tricyanomelaminate ions, respectively. On the other hand, the series of signals in the region 1300–1600 $cm^{-1}$ and the weak band at 970 $cm^{-1}$ as well as the sharp signal at 786 $cm^{-1}$ can be attributed to the stretching and bending vibrations of the triazine rings, respectively. The broad band between 3600 and 3200 $cm^{-1}$ can be attributed to the stretching vibrations of water molecules. Furthermore, in contrast to non-protonated tricyanomelaminate, more significant signals are observed between 2800 and 3200 $cm^{-1}$ in the case of LnTCM. These signals may be assigned to N−H···N stretching vibrations ($\nu$NH), indicating the presence of protonated tricyanomelaminate as well as $[NH_4]^+$ ions in LnTCM.[50]

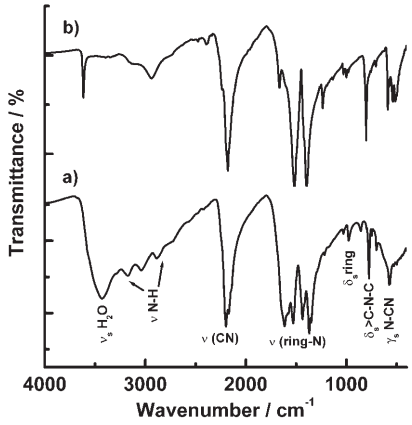


Figure 1. Infrared spectra of a) $[NH_4]La[HC_6N_9]_2[H_2O]_7 \cdot H_2O$ and b) $Na_3[C_6N_9] \cdot 3H_2O$.

**Solid-state MAS NMR studies**: The X-ray crystal structure of LaTCM is not very specific with regard to the location of hydrogen atoms due to the weak scattering factor of hydrogen. For this reason, it is not clear from the X-ray diffraction analysis alone how the charge balance is achieved in LaTCM. Moreover, there is the possibility of hydrogen bonding, which might "tie up" the protonated tricyanomelaminate leading to a stable structure. Thus, it is also of interest to study the effect of temperature on the crystal structure. Therefore, $^1H$, $^{15}N$, and $^{13}C$ solid-state MAS NMR spectroscopy were chosen as a sensitive probe to elucidate the structural network of diamagnetic lanthanum tricyanomelaminate (LaTCM). For insensitive nuclei such as $^{15}N$ and $^{13}C$, MAS NMR spectra were recorded using the cross-polarization technique to prove spatial proximity. This is only possible if the motion of the hydrogen atoms on the NMR time scale can be neglected. For this reason, we also carried out a qualitative variable-temperature study.

**$^1$H MAS NMR spectroscopy**: A $^1H$ MAS NMR spectrum of LaTCM spun at 30 kHz reveals four proton resonances at $\delta = 5.6$, 7.6, 11.1, and 12.8 ppm (Figure 2). The observed chemical shifts can be tentatively assigned to the isotropic chemical shifts of $\delta_{iso}(H_2O)$ ($\delta = 5.6$ ppm), $\delta_{iso}(NH_4^+)$ ($\delta = 7.6$ ppm), and $\delta_{iso}(N{-}H)$ ($\delta = 11.1$ and 12.8 ppm). The $\delta_{iso}(NH_4^+)$ of 7.6 ppm is in agreement with the $^1H$ chemical shifts of the ammonium ion found in other compounds, which are also around $\delta = 7$ ppm, for example, $\delta = 7.1$ ppm in solid $NH_4Cl$, $\delta = 6.9$ ppm in $NH_4HSO_4$, and $\delta = 7.2$ ppm in $NH_4H_2PO_4$. Thus, the $^1H$ MAS NMR spectrum gives an initial indication of the presence of $[NH_4]^+$, protonated tricyanomelaminate, and water molecules in LaTCM.

It is well known that hydrogen bonds become weaker at elevated temperatures and can lead to ionic conduction. A direct effect of hydrogen motion is that anisotropic properties are averaged on the NMR time scale. Figure 3 shows the effect of temperature on the $^1H$ MAS NMR spectrum. At room temperature, a multitude of rotational spinning sidebands is seen, whereas at higher temperatures

  

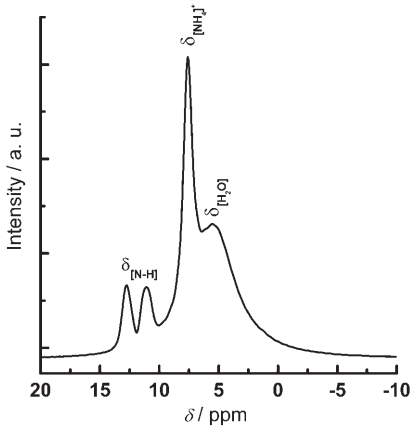


Figure 2. $^1$H MAS NMR spectrum of $[NH_4]La[HC_6N_9]_2[H_2O]_7{\cdot}H_2O$ obtained at a spinning frequency of 30 kHz. Hydrogen background suppression was realized by means of a DEPTH experiment.[55]

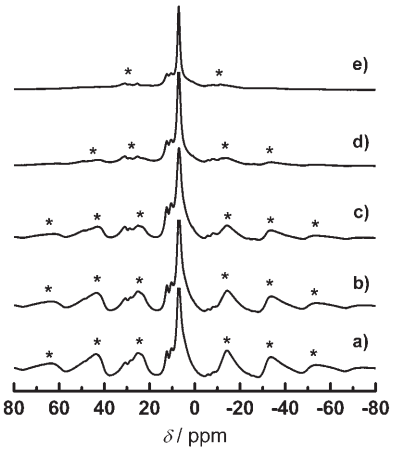


Figure 3. Temperature-dependent $^1$H solid-state MAS NMR spectra of $[NH_4]La[HC_6N_9]_2[H_2O]_7{\cdot}H_2O$ recorded at: a) −1 °C, b) 31 °C, c) 53 °C, d) 95 °C, and e) 121 °C. The asterisks indicate the spinning sidebands. Almost identical spectra in a) and b) indicate that dipolar interactions are hardly affected by the slow proton mobility at room temperature.

(≈120 °C), hydrogen motion leads to suppression of these rotational spinning sidebands. The sidebands are dominated by the homonuclear magnetic dipole–dipole interaction of two hydrogen atoms in a water molecule, with a dipole–dipole coupling constant of approximately −32 kHz. Therefore, it can be concluded that, at room temperature, hydrogen motion that would lead to significant averaging of the dipolar interactions may be neglected, indicating that the cross-polarization experiments can be discussed with reference to a static model of the atom arrangement.

**$^1$H 2D double-quantum single-quantum (DQ SQ) correlation MAS NMR spectrum** (Figure 4): In 2D DQ experiments, only hydrogen atom pairs that are in close proximity give rise to a double-quantum filtered signal. Hydrogen atom pairs having equivalent chemical shifts give on-diagonal peaks, whereas those pairs with different chemical shifts result in off-diagonal peaks. Therefore, on-diagonal signals

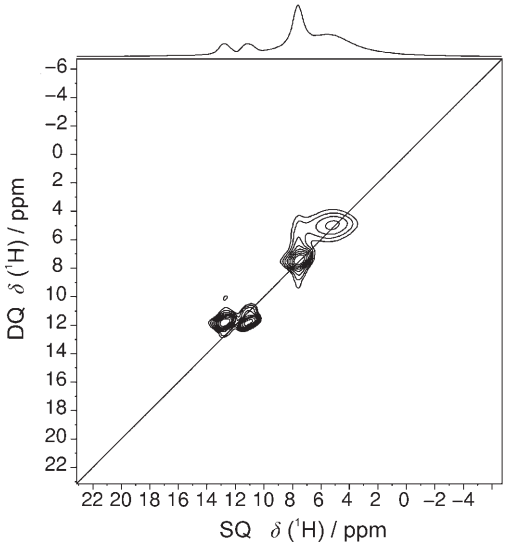


Figure 4. $^1$H 2D DQ SQ correlation spectrum of $[NH_4]La[HC_6N_9]_2[H_2O]_7{\cdot}H_2O$ at a spinning frequency of 30 kHz, obtained using the BABA pulse sequence.[56] The spectrum at the top is the 1D SQ spectrum of $^1$H as shown in Figure 2. Hydrogen atoms in N−H···N bonds give rise to off-diagonal correlation peaks at 11.1 and 12.8 ppm.

are expected from the hydrogen atoms of $H_2O$ molecules and $[NH_4]^+$ ions, since different water and ammonium peaks cannot usually be resolved in $^1$H solid-state MAS NMR. On the other hand, the double-quantum signals of hydrogen-bonded hydrogen atoms (N−H···N) are expected to be off-diagonal because of the non-equivalent chemical shifts of these nuclei arising from two crystallographically independent monoprotonated tricyanomelaminate anions in LaTCM. From the assignments, the shortest distance between unlike spin pairs, H1···H10, can be estimated to be 2.6 Å, while the distances between like spin pairs, H1···H1 and H10···H10, are longer at 4.2 and 4.3 Å, respectively. Thus, it can be concluded that the 2D DQ experiments are wholly consistent with the previous assignment of the $^1$H MAS NMR peaks (Figure 2).

**$^{13}$C CP MAS NMR spectroscopy**: The $^{13}$C CP MAS NMR spectrum of LaTCM shows a series of signals in the region between $\delta = 110$ and 175 ppm (Figure 5). The resonances observed in the high-field region ($\delta = 118$–127 ppm) can be attributed to the sp-hybridized C≡N groups of the N−C≡N units (Figure 5 (inset); Scheme 2). These $^{13}$C NMR chemical shifts are similar to that of the cyanamide carbon atoms in the N−C≡N units of potassium melonate ($\delta = 124.8$ ppm).[24] Moreover, the cyanamide chemical shifts in LaTCM are comparable with those in organic cyanides such as acetamide ($\delta = 116.8$ ppm), propionitrile ($\delta = 120.8$ ppm), and benzonitrile ($\delta = 118.7$ ppm). The presence of multiple signals indicates more than one chemically nonequivalent position for the N−C≡N units, which is consistent with the crystal structure analysis that showed two different tricyanomelaminate moieties. The $^{13}$C MAS NMR signals at around $\delta =$ 163 and 172 ppm can be attributed to the triazine core of

  

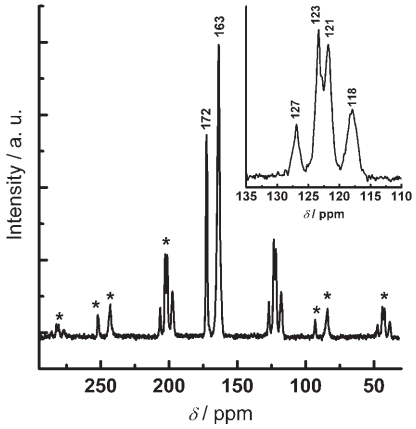


Figure 5. $^{13}C$ CP MAS NMR spectrum of $[NH_4]La[HC_6N_9]_2[H_2O]_7{\cdot}H_2O$. The inset shows an enlargement of the spectrum from $\delta = 110$ to 135 ppm. The asterisks indicate the spinning sidebands.

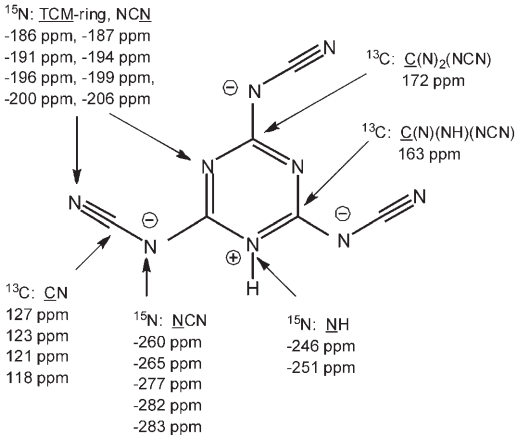


Scheme 2. $^{13}C$ and $^{15}N$ chemical shifts observed for $[NH_4]La[HC_6N_9]_2[H_2O]_7{\cdot}H_2O$.

the tricyanomelaminate moieties. According to the literature, the $CN_2(NH_2)$ carbon atoms in melamine give rise to two signals at $\delta = 167.5$ and 169.2 ppm, while in melem the corresponding signals are observed at around $\delta = 164.3$ and 166.4 ppm.[7] In contrast, the signals of the $CN_2X$ carbon atoms (X = Cl, N–C≡N) in 2,5,8-trichloro-tri-*s*-triazine ($C_6N_7Cl_3$)[57] and in potassium melonate ($K_3[C_6N_7(NCN)_3]{\cdot}5H_2O$)[25] are shifted to lower field ($\delta = 175$ and 174.3 ppm, respectively). By comparison with these previous studies, it can be postulated that there are two types of carbon atom environment in the triazine ring of LaTCM, indicating the presence of monoprotonated $[HC_6N_9]^{2-}$ ions. Therefore, the $^{13}C$ signals at $\delta = 163$ and 172 ppm may be assigned to the [*C*(N)(NH)(NCN)] and [*C*(N)$_2$(NCN)] carbon atoms of the $[HC_6N_9]^{2-}$ ions, respectively (Scheme 2).

**$^{15}N$ CP and CPPI MAS NMR spectroscopy**: A $^{15}N$ MAS NMR study was performed on LaTCM using both cross-polarization (CP) and cross-polarization combined with polarization-inversion (CPPI) techniques (Figure 6). The $^{15}N$ CP

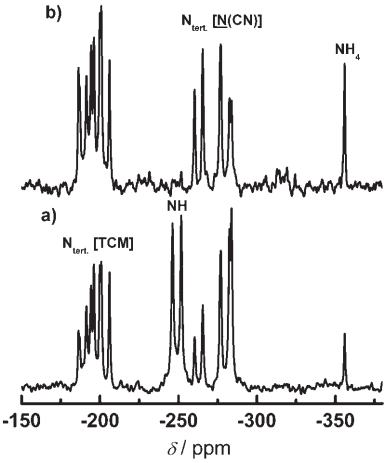


Figure 6. $^{15}N$ MAS solid-state NMR spectra of $[NH_4]La[HC_6N_9]_2[H_2O]_7{\cdot}H_2O$ recorded using a) cross-polarization (CP), and b) cross-polarization combined with polarization-inversion (CPPI) techniques.

MAS NMR spectrum shows chemical shifts between $\delta = -180$ and $-350$ ppm (Figure 6a). The sharp resonance at $\delta = -356$ ppm can be assigned to a tetracoordinate nitrogen atom and is in good agreement with the chemical shifts for $[NH_4]^+$ in other compounds.[10] The resonances of the *N*–C≡N nitrogen atoms are observed between $\delta = -260$ and $-283$ ppm (Scheme 2). These values compare well with the *N*–C≡N signals in ammonium tricyanomelaminate ($[NH_4]_2[HC_6N_9]$), guanidinium tricyanomelaminate ($[C(NH_2)_3]_3[C_6N_9]{\cdot}2H_2O$), and melaminium tricyanomelaminate ($[C_3N_6H_7]_2[HC_6N_9]{\cdot}2.4H_2O$).[10] To verify that the observed signal was not due to the by-product $NH_4Cl$ or the starting material ammonium tricyanomelaminate ($[NH_4]_2[HC_6N_9]$), which might have been present as impurities in the bulk LaTCM, $^{15}N$ CP MAS NMR spectra were recorded for $NH_4Cl$ and $[NH_4]_2[HC_6N_9]$ under the same conditions. The $^{15}N$ signal of $[NH_4]^+$ in $NH_4Cl$ was found to appear at $\delta = -341$ ppm, whereas that of LaTCM appears at $\delta = -356$ ppm. This excludes the possibility of the presence of $NH_4Cl$ as an impurity phase. Similarly, $[NH_4]_2[HC_6N_9]$ shows two signals between $\delta = -340$ and $-350$ ppm due to the presence of two crystallographically independent $[NH_4]^+$ moieties, which therefore also rules out possible contamination with this compound.[10] The signals in the range $\delta = -186$ to $-206$ ppm are assigned to the ring nitrogen atoms of the *s*-triazine cycle and the cyanamide units of the N–C≡N side arms. These chemical shifts are in good agreement with those of other carbon–nitride compounds containing *s*-triazine cores.[7,10] The multiple splitting of signals originating from the *N*–C≡N, N–C≡*N*, and *s*-triazine ring nitrogen atoms indicates that more than one nonequivalent tricyanomelaminate ion is present in the crystal structure of LaTCM. The resonances observed at $\delta = -246$ and $-251$ ppm are assigned to the protonated NH groups of the $[HC_6N_9]^{2-}$ ions. The appearance of two signals reflects the presence of two distinct NH groups arising from two mo-

  

noprotonated tricyanomelaminate moieties. This has been further confirmed through a CPPI experiment (Figure 6b).

CPPI experiments permit the identification of $^{15}N$ sites according to their proton environments. In other words, one can distinguish between $NH_2$ groups, NH groups, and tertiary N atoms bearing no proton.[58] During the sequence, the magnetization starts from a maximum value. In the case of NH and $NH_2$, it decreases and becomes negative with increasing inversion time. The theoretical normalized polarization inversion curves for the $NH_n$ groups are dominated by two regimes, the crossover between which is observable at a normalized intensity given by $[2/(n+1)]-1$ ($n=0,1,2$). However, the magnetization behavior of an $NH_3$ or $NH_4$ group can be adequately described by a single exponential regime, which is also the case for a non-protonated nitrogen. For the particular inversion time chosen in this experiment (160 μs), the normalized intensity of the NH groups (crossover at 0) is expected to be zero.[7] Thus, comparison of the polarization transfer dynamics using the CPPI sequence should allow a clear distinction of the NH sites on the basis of the various time constants related to the polarization inversion dynamics. As demonstrated in Figure 6b, the experimental intensities corresponding to the NH moieties are significantly lowered compared to the magnetization of the other signals, thus confirming the presence of two chemically nonequivalent NH groups. Therefore, the CP and CPPI $^{15}N$ MAS NMR studies indicate the presence of $[NH_4]^+$ ions as well as two NH groups belonging to two crystallographically independent monoprotonated tricyanomelaminate moieties, revealing the formula unit of $[NH_4]Ln[HC_6N_9]_2[H_2O]_7{\cdot}H_2O$ to be one in which $[NH_4]^+$ and $Ln^{3+}$ ions function as charge-compensating cations for two monoprotonated $[HC_6N_9]^{2-}$ ions.

**$^{15}N\{^1H\}$ 2D CP heteronuclear correlation (HETCOR) MAS NMR spectroscopy**: Rotor-synchronized 2D $^{15}N\{^1H\}$ CP HETCOR experiments permit the study of spatial proximity between hydrogen and nitrogen atoms. We chose two different contact times for our experiments. At short contact times, dipolar coupling can only take place between the nitrogen and hydrogen atoms that are in close proximity, whereas at long contact times, the nitrogen atoms can interact with all protons in the crystal structure. A 2D spectrum obtained with a short contact time (2 ms) shows only the signals of N–H···N hydrogen-bonded atoms (Figure 7). The absence of an ammonium ion signal indicates that the strong dipolar contacts between the nitrogen and hydrogen atoms within an $[NH_4]^+$ ion result in a reduced contribution to the CP signal due to rotational motion. Two different N–H···N moieties are resolved, which is consistent with the results of the CP and CPPI experiments, and these can be assigned to the strong hydrogen bonds within the LaTCM dimer. The spectrum obtained with a long contact time (10 ms), on the other hand, shows peaks between almost all of the hydrogen and nitrogen atoms present in the same crystallographic phase (Figure 8). Figure 8 (inset) shows the correlation signals between the nitrogen atom of the $[NH_4]^+$ ion and the other hydrogen atoms in the crystal structure, indicating that all peaks stem from the same crystallographic phase.

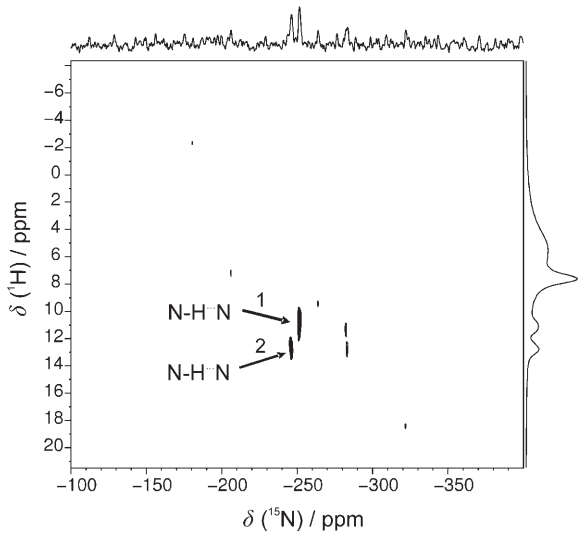


Figure 7. $^{15}N\{^1H\}$ 2D CP HETCOR MAS NMR spectrum of $[NH_4]La[HC_6N_9]_2[H_2O]_7{\cdot}H_2O$ recorded with a contact time of 2 ms. The spectrum at the top is the 1D $^{15}N$ CP MAS NMR spectrum, while that at the right is the 1D $^1H$ MAS NMR spectrum. Two distinct N–H···N hydrogen bonds are resolved.

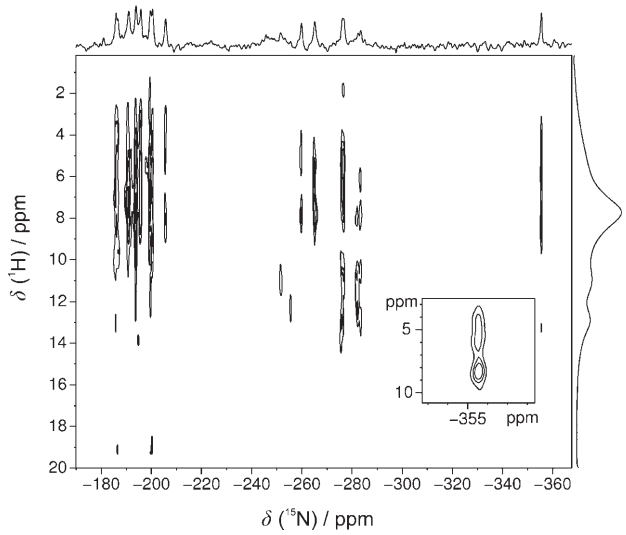


Figure 8. $^{15}N\{^1H\}$ 2D CP HETCOR MAS NMR spectrum of $[NH_4]La[HC_6N_9]_2[H_2O]_7{\cdot}H_2O$ recorded with a contact time of 10 ms. The inset shows an expansion of the ammonium signals from $\delta=-352$ to $-359$ ppm. The spectrum at the top is the 1D $^{15}N$ CP MAS NMR spectrum, while that at the right is the 1D $^1H$ MAS NMR spectrum.

**Crystal structure**: The crystal structure of $[NH_4]La[HC_6N_9]_2[H_2O]_7{\cdot}H_2O$ was solved from single-crystal X-ray diffraction data, and the assignments of the ammonium ions and monoprotonated tricyanomelaminate moieties were derived from solid-state MAS NMR studies. The structure was found to be built up of $La^{3+}$ and two crystallographically independent monohydrogentricyanomelaminate ions

  

$[HC_6N_9]^{2-}$, ammonium ions, and crystal water molecules (Figure 9). Details of the structure refinement are summarized in Table 1. The atomic coordinates, anisotropic displacement parameters, and bond lengths and angles of LaTCM are given in the Supporting Information. The monoprotonated $[HC_6N_9]^{2-}$ ions are planar and are oriented approximately perpendicular to the *a* axis [100] (Figure 10).

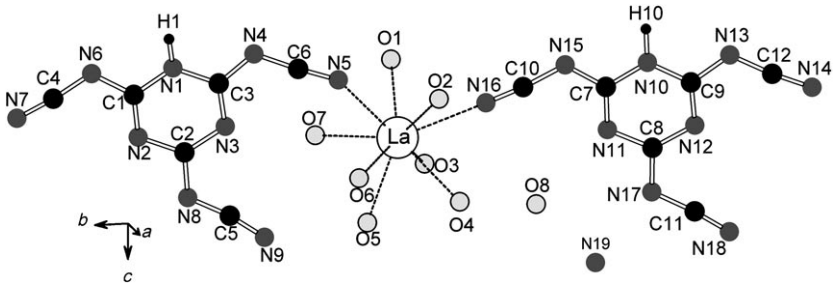


Figure 9. Representation of one formula unit of the unit cell of $[NH_4]La[HC_6N_9]_2[H_2O]_7{\cdot}H_2O$ showing the coordination mode of $La^{3+}$. The hydrogen atoms of the $[NH_4]^+$ group and water molecules have been omitted.

Table 1. Crystallographic data for LaTCM ($[NH_4]La[HC_6N_9]_2[H_2O]_7{\cdot}H_2O$).

| | |
|---|---|
| formula | $[NH_4]La[HC_6N_9]_2[H_2O]_7{\cdot}H_2O$ |
| molecular weight [g mol$^{-1}$] | 699.24 |
| crystal system | triclinic |
| space group | $P\bar{1}$ |
| diffractometer | STOE IPDS single crystal |
| wavelength $\lambda$ [Å] | $Mo_{K\alpha}$, 0.71073 |
| temperature [K] | 293 |
| twin law | $\begin{pmatrix} 1 & 0 & 0 \\ 0.182 & -1 & 0 \\ 0.826 & 0 & -1 \end{pmatrix}$ |
| $a$ [Å] | 7.1014(14) |
| $b$ [Å] | 13.194(3) |
| $c$ [Å] | 13.803(3) |
| $\alpha$ [°] | 90.11(3) |
| $\beta$ [°] | 77.85(3) |
| $\gamma$ [°] | 87.23(3) |
| V [Å$^3$] | 1262.7(5) |
| $Z$ | 2 |
| $\rho_{calcd}$ [g cm$^{-3}$] | 1.786 |
| $F(000)$ | 656 |
| $\mu$ [mm$^{-1}$] | 1.769 |
| crystal size [mm$^3$] | $0.19\times0.18\times0.17$ |
| diffraction range | $2.94 \leqq \theta \leqq 30.46$ |
| index range | $-9 \leqq h \leqq 9$, $-18 \leqq k \leqq 18$, $-19 \leqq l \leqq 19$ |
| total number of reflections | 11 109 |
| independent reflections | 5553 ($R_{int}=0.0909$) |
| observed reflections | 3186 |
| refined parameters | 367 |
| absorption correction | multi scan |
| min./max. transmission ratio | 0.875/0.956 |
| min./max. residual electron density [e Å$^{-3}$] | −0.844/0.867 |
| GOF | 1.040 |
| final $R$ indices [$I>2\sigma(I)$][a] | $R1=0.0627$, $wR2=0.1588$ |
| R indices (all data)[a] | $R1=0.1176$, $wR2=0.1814$ |

[a] $w=[\sigma^2(F_o^2) + (0.0772P)^2 + 0.0000P]^{-1}$, where $P=(F_o^2 + 2F_c^2)/3$.

One of the three side arms of the $[HC_6N_9]^{2-}$ ion is differently oriented, reducing the idealized symmetry of the molecular anion from $C_{3h}$ to approximately $C_s$. This type of arrangement of the $[HC_6N_9]^{2-}$ motifs may be attributed to the steric requirements of the proton with respect to the adjacent cyanamide moieties, as has been observed in other compounds containing monoprotonated tricyanomelaminate ions.[10,49] Although tricyanomelaminate compounds with nonprotonated $[C_6N_9]^{3-}$ moieties possessing $C_s$ symmetry are known,[35,37] the latter point symmetry could be enforced by the proton attached to the triazine ring between two cyanamide moieties in $[HC_6N_9]^{2-}$, which would then allow the two side arms of N4-C6-N5 and N8-C5-N9 as well as N13-C12-N14 and N17-C11-N18 to adopt an almost mutually parallel arrangement so as to reduce steric hindrance. The $[HC_6N_9]^{2-}$ moieties in LaTCM form parallel layers perpendicular to [100], with an interlayer stacking distance of approximately 3.6 Å. The hydrogen atoms H1 and H10 are bound to the triazine ring nitrogen atoms N1 and N10, respectively.

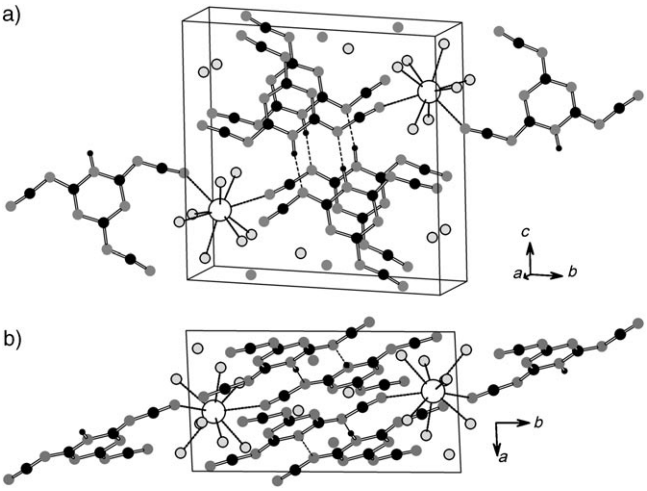


Figure 10. Views along a) the *a* axis, showing hydrogen bonding between two tricyanomelaminates, and b) the *c* axis of the unit cell of $[NH_4]La[HC_6N_9]_2[H_2O]_7{\cdot}H_2O$, showing the parallel stacking of $[HC_6N_9]^{2-}$ moieties perpendicular to the *a* axis. The hydrogen atoms of the $[NH_4]^+$ group and water molecules have been omitted.

In the crystal structure of LaTCM, each $La^{3+}$ ion is surrounded by two nitrogen atoms from two different tricyanomelaminate moieties and seven oxygen atoms from crystal water molecules, forming nine-coordinated heptagonal-bipyramidal $LaN_2O_7$ polyhedra. The $[HC_6N_9]^{2-}$ ions are coordinated to $La^{3+}$ through their terminal nitrogen atoms N5

  

and N16. The La–O distances range from 2.52 to 2.62 Å, which are comparable to those in lanthanum oxide compounds. Furthermore, the La–N distances are between 2.62 and 2.69 Å, which is in good agreement with that in lanthanum dicyanamide.[44]

In the $[HC_6N_9]^{2-}$ ions, the C–N distances range from 1.29 to 1.37 Å, except for those involving the terminal nitrogen atoms (1.13–1.16 Å), the latter representing terminal C≡N bonds. The angles within the N–C≡N side arms are almost linear (171–175°). The respective values are comparable to those found in other monoprotonated ($M^{II}[HC_6N_9]\cdot 3H_2O$, $[NH_4]_2[HC_6N_9]$, and $[C_3N_9H_7]_2[HC_6N_9]\cdot 2.4H_2O$),[10,50] diprotonated ($Co[H_2C_6N_9][H_2O]_4\cdot 6H_2O$ and $Rb[H_2C_6N_9]\cdot 0.5H_2O$),[51,52] and non-protonated ($M_3[C_6N_9]$; M = Na, K, Rb)[35,37,49] tricyanomelaminate compounds.

In the crystal structure of LaTCM, intermolecular hydrogen bonds are observed between the protonated ring atoms and the cyanamide side-arms of adjacent $[HC_6N_9]^{2-}$ moieties (N1–H1···N15 and N10–H10···N6), giving rise to an eight-membered ring-type arrangement, and thereby forming a tricyanomelaminate dimer (Figure 10). This is in good agreement with the $^1H$ and $^{15}N$ MAS NMR spectra. Moreover, though the hydrogen atoms of the water molecules could not be unequivocally determined, the distances between the nitrogen atoms of the tricyanomelaminate moieties and the oxygen atoms of the water molecules coordinated to $La^{3+}$ (O–H···N = 2.7–3.2 Å) indicate that each water molecule in the $LaN_2O_7$ polyhedra is involved in at least one hydrogen bond with the nitrogen atom of an N–C≡N side arm of an $[HC_6N_9]^{2-}$ ion. On the other hand, the water molecule that is not coordinated to $La^{3+}$ may be involved in hydrogen bonds to a nitrogen atom of a triazine ring (O8–H···N11 2.93 Å), a terminal nitrogen atom (O8–H···N16 3.39 Å), and the nitrogen atom of the $[NH_4]^+$ ion (O8–H···N19 2.93 Å). Furthermore, the $[NH_4]^+$ nitrogen atom can also show hydrogen bonding to a nitrogen atom of an N–C≡N side-arm (N19–H···N17), as was evident from the $^{15}N\{^1H\}$ 2D CP HETCOR MAS NMR spectrum.

Owing to the similarity of the X-ray powder patterns, the eight phases of $[NH_4]Ln[HC_6N_9]_2[H_2O]_7\cdot H_2O$ (Ln = Ce, Pr, Nd, Sm, Eu, Gd, Tb, Dy) could be indexed with the same space group as $[NH_4]La[HC_6N_9]_2[H_2O]_7\cdot H_2O$. Therefore, with reference to the structural model of LaTCM, the structures of the other eight rare-earth tricyanomelaminates, LnTCM (Ln = Ce, Pr, Nd, Sm, Eu, Gd, Tb, Dy) were refined by the Rietveld method with the program GSAS,[59] using the lattice parameters and the atomic coordinates of LaTCM as the starting values. Figure 11 shows the Rietveld plot of GdTCM ($[NH_4]Gd[HC_6N_9]_2[H_2O]_7\cdot H_2O$). The Rietveld plots of the other LnTCM compounds (Ln = Ce, Pr, Nd, Sm, Eu, Tb, Dy) are given in Figures S1–S7 in the Supporting Information. To describe the profile of the X-ray reflections, a pseudo-Voigt function was used.[60,61] Details of the structure determination are summarized in Table 2. It can be seen from Table 2 that the lattice parameters and volumes of the triclinic unit cells of LnTCM (Ln = La, Ce, Pr, Nd, Sm, Eu, Gd, Tb, Dy) decrease with decreasing ionic radius of the rare-earth ions owing to the lanthanide contraction.

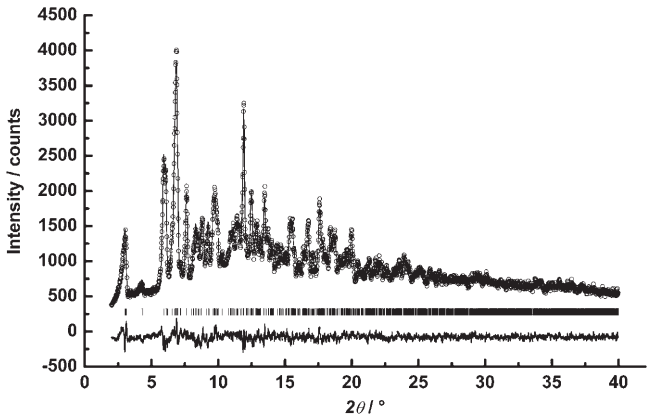


Figure 11. Final Rietveld refinement plot for $[NH_4]Gd[HC_6N_9]_2[H_2O]_7\cdot H_2O$. Observed (open circles), calculated (line), and the difference profile of the X-ray powder diffraction are plotted on the same scale. Bragg peaks for this compound are indicated by vertical lines.

**Photoluminescence studies**: Photoluminescence studies were carried out on europium tricyanomelaminate ($[NH_4]Eu[HC_6N_9]_2[H_2O]_7\cdot H_2O$) and terbium tricyanomelaminate ($[NH_4]Tb[HC_6N_9]_2[H_2O]_7\cdot H_2O$). Figure 12 shows the excitation-emission spectra of EuTCM. The excitation spectrum monitored at 615 nm shows a series of sharp lines between 300 and 550 nm attributable to $Eu^{3+}$ intra-4f transitions.[62] Unlike other $Eu^{3+}$ compounds, EuTCM does not show the typical Eu–N charge-transfer band in the excitation spectrum.[54] This indicates that the Eu–N charge-transfer band in EuTCM might be situated at much higher energy such that it cannot participate in the excitation process. The diffuse reflectance spectrum also shows absorptions corresponding to the intra-4f $Eu^{3+}$ levels in EuTCM. Moreover, the broad band in the UV region with a maximum at 285 nm can be attributed to the tricyanomelaminate moieties. The broad spectrum is comparable to the absorption band observed in the case of sodium tricyanomelaminate (see Figure S8 in the Supporting Information). The emission spectrum of EuTCM, recorded at $\lambda_{exc} = 397$ nm, is composed of the typical $Eu^{3+}$ intra-$^4f_6$ emission lines, which can be assigned to transitions between the first excited state ($^5D_0$) and the ground multiplets ($^7F_{1-4}$).[62] Furthermore, the $^5D_0$–$^7F_1$ line is known to originate from a magnetic dipole transition, while the $^5D_0$–$^7F_2$ line originates from an electric dipole transition.[63] According to the Judd–Ofelt theory,[64,65] the magnetic dipole transition is permitted while the electric dipole transition is forbidden. The latter is only allowed under the condition that the $Eu^{3+}$ ions occupy a site without an inversion center and are sensitive to local symmetry. In the case of EuTCM, the electric dipole transition is much stronger than the magnetic dipole transition, suggesting that the $Eu^{3+}$ occupies a low-symmetry site without an inversion center.

  

Table 2. Crystallographic data for the other eight LnTCM compounds.

| $(NH_4)Ln(HC_6N_9)_2(H_2O)_7{\cdot}H_2O$ | Ln = Ce | Ln = Pr | Ln = Nd | Ln = Sm | Ln = Eu | Ln = Gd | Ln = Tb | Ln = Dy |
|---|---|---|---|---|---|---|---|---|
| formula weight | 700.45 | 701.24 | 704.20 | 710.69 | 712.30 | 717.58 | 719.20 | 722.83 |
| crystal system | triclinic | triclinic | triclinic | triclinic | triclinic | triclinic | triclinic | triclinic |
| space group | $P\bar{1}$ (no. 2) | $P\bar{1}$ (no. 2) | $P\bar{1}$ (no. 2) | $P\bar{1}$ (no. 2) | $P\bar{1}$ (no. 2) | $P\bar{1}$ (no. 2) | $P\bar{1}$ (no. 2) | $P\bar{1}$ (no. 2) |
| radiation ($\lambda$ [Å]) | $Mo_{K\alpha1}$ (0.7093) | $Mo_{K\alpha1}$ (0.7093) | $Mo_{K\alpha1}$ (0.7093) | $Mo_{K\alpha1}$ (0.7093) | $Mo_{K\alpha1}$ (0.7093) | $Mo_{K\alpha1}$ (0.7093) | $Mo_{K\alpha1}$ (0.7093) | $Mo_{K\alpha1}$ (0.7093) |
| lattice parameters | | | | | | | | |
| $a$ [Å] | 7.05930(32) | 7.04289(32) | 7.03326(31) | 7.00694(32) | 6.9863(5) | 6.9783(5) | 6.9683(5) | 6.9546(12) |
| $b$ [Å] | 13.1318(8) | 13.1245(8) | 13.1200(7) | 13.1034(7) | 13.0803(13) | 13.0777(12) | 13.0770(10) | 13.0780(29) |
| $c$ [Å] | 13.7247(8) | 13.6925(8) | 13.6755(7) | 13.6306(7) | 13.5869(13) | 13.5779(12) | 13.5603(11) | 13.5417(31) |
| $\alpha$ [°] | 90.097(4) | 90.159(4) | 90.153(4) | 90.188(4) | 90.225(7) | 90.257(6) | 90.262(5) | 90.271(14) |
| $\beta$ [°] | 77.959(4) | 78.125(4) | 78.262(4) | 78.515(4) | 78.616(7) | 78.680(6) | 78.811(5) | 78.934(13) |
| $\gamma$ [°] | 87.109(4) | 87.070(4) | 87.039(4) | 86.9880(35) | 86.995(6) | 86.930(6) | 86.902(5) | 86.880(13) |
| $V$ [Å$^3$] | 1242.63(12) | 1236.84(12) | 1233.78(11) | 1224.61(11) | 1215.38(19) | 1213.13(18) | 1210.27(16) | 1206.8(4) |
| $Z$ | 2 | 2 | 2 | 2 | 2 | 2 | 2 | 2 |
| $\rho_{calcd}$ [g cm$^{-3}$] | 1.819 | 1.829 | 1.843 | 1.873 | 1.892 | 1.910 | 1.919 | 1.934 |
| profile range | $2 \leqq \theta \leqq 40$ | $2 \leqq \theta \leqq 40$ | $2 \leqq \theta \leqq 40$ | $2 \leqq \theta \leqq 40$ | $2 \leqq \theta \leqq 40$ | $2 \leqq \theta \leqq 40$ | $2 \leqq \theta \leqq 40$ | $2 \leqq \theta \leqq 40$ |
| profile parameters | 19 | 19 | 19 | 19 | 19 | 19 | 19 | 19 |
| $R$ values | | | | | | | | |
| $wR_p$ (fitted) | 0.0435 | 0.0355 | 0.0419 | 0.0391 | 0.0631 | 0.0450 | 0.0439 | 0.0453 |
| $wR_p$ (background) | 0.0438 | 0.0365 | 0.0332 | 0.0405 | 0.0402 | 0.0456 | 0.0485 | 0.0522 |
| $R_p$ (fitted) | 0.0343 | 0.0284 | 0.0433 | 0.0300 | 0.0282 | 0.0352 | 0.0338 | 0.0341 |
| $R_p$ (background) | 0.0348 | 0.0292 | 0.0342 | 0.0296 | 0.0291 | 0.0356 | 0.0357 | 0.0364 |
| $R_F^2$ | 0.0886 | 0.0838 | 0.1019 | 0.0602 | 0.0830 | 0.0693 | 0.0885 | 0.0854 |

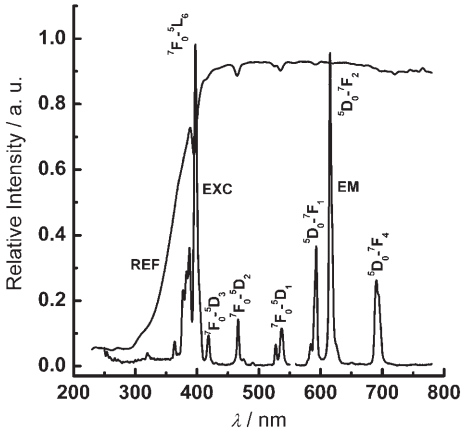


Figure 12. The diffuse reflectance (REF), excitation (EXC), and emission (EM) spectra of $[NH_4]Eu[HC_6N_9]_2[H_2O]_7{\cdot}H_2O$ at room temperature. The excitation and emission spectra were recorded at $\lambda_{em} = 615$ nm and $\lambda_{exc} = 397$ nm, respectively.

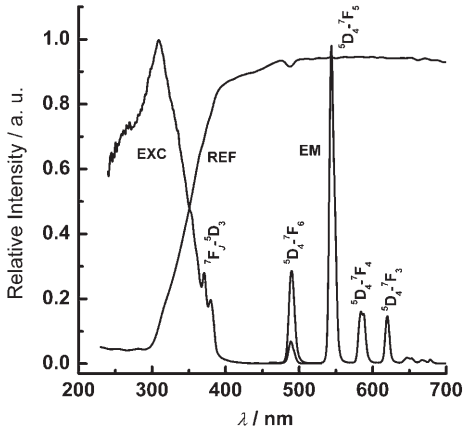


Figure 13. The diffuse reflectance (REF), excitation (EXC), and emission (EM) spectra of $[NH_4]Tb[HC_6N_9]_2[H_2O]_7{\cdot}H_2O$ at room temperature. The excitation and emission spectra were recorded at $\lambda_{em} = 545$ nm and $\lambda_{exc} = 310$ nm, respectively.

The excitation spectrum of TbTCM, monitored at the $Tb^{3+}$ green emission at 545 nm ($^5D_4$–$^7F_5$), mainly consists of a wide band between 240 and 400 nm with a maximum at 300 nm, superimposed with sharp lines at around 370 and 380 nm, and a further sharp line at 488 nm (Figure 13). The diffuse reflectance spectrum also shows a sharp absorption at 488 nm and a broad band at 300 nm. The sharp lines originate from intra-4f transitions of $Tb^{3+}$. The broad band can be assigned to the $^4f_8$–$^4f_7$5d transition of $Tb^{3+}$.[62] In fluoro and oxo compounds, the $^4f_8$–$^4f_7$5d transition of $Tb^{3+}$ is generally observed at relatively higher energy. In the present case, a shift of the f–d transitions to lower energies can be expected due to the nephelauxetic effect. Excitation of the $^4f_8$–$^4f_7$5d transition of $Tb^{3+}$ at 300 nm yields the characteristic $^5D_4$–$^7F_J$ ($J = 3$–6) emission of $Tb^{3+}$, with $^5D_4$–$^7F_5$ green emission as the most intense band ($\lambda_{max} = 545$ nm).

The CIE (Commission Internationale d'Eclairage) color coordinates ($x$, $y$) of EuTCM (0.618, 0.362) and TbTCM (0.325, 0.575) are quite comparable to those of commercial red- and green-emitting phosphors, respectively. Quantum efficiencies have been measured at a monitoring wavelength of 365 nm in order to compare EuTCM and TbTCM with standard lamp phosphors. The quantum efficiencies (QE) described here are overall quantum efficiencies of the luminescent materials.[66] For EuTCM, lumogen red, a perylene dye (BASF) with QE = 0.42 for 365 nm excitation, was used as a reference. At this excitation wavelength, EuTCM shows QE = 0.06. In the case of TbTCM, commercial $LaPO_4$:Ce,Tb

  

powder (Philips Lighting Components) with QE = 0.28 and $SrSi_2N_2O_2$:Eu (laboratory standard) with QE = 0.81 for 365 nm excitation were used as references. At an excitation wavelength of 365 nm, TbTCM shows QE = 0.18.

**Thermal behavior**: The thermal stability of $[NH_4]Ln[HC_6N_9]_2[H_2O]_7{\cdot}H_2O$ has been studied by means of thermogravimetric analysis (TG/DTA). Since LnTCM contains water molecules, structural changes at higher temperatures are expected for this compound. TG/DTA measurements performed on LnTCM between 20 and 800 °C showed nearly identical results for all of the compounds, with three weight losses (Figure 14). The initial weight loss of 21 % in the region from 100 to 150 °C, accompanied by an endothermic DTA signal at 150 °C, most likely corresponds to the loss of adsorbed water, ammonia, and lattice water. This is also quite consistent with the results of our temperature-dependent $^1H$ MAS NMR studies, in which proton signals corresponding to $[NH_4]^+$, $H_2O$, and N–H moieties were found to persist even up to 120 °C. The thermal behavior observed by temperature-programmed X-ray diffractometry (TPXRD) is also in accordance with the thermoanalytical analyses, showing the conversion of hydrated lanthanum tricyanomelaminate to another crystalline phase at 150 °C (see Figure S9 in the Supporting Information). This crystalline phase might indicate the formation of dehydrated lanthanide tricyanomelaminates containing significantly less crystal water as compared to the initial hydrated phase. The crystallinity of the compound is retained in the dehydrated phase. These observations are corroborated by infrared spectroscopy (see Figure S10 in the Supporting Information). After annealing the sample at 150 °C, the vibrational characteristics remain unchanged except for a diminution in the broad band in the region 3600–3200 $cm^{-1}$ due to O–H stretching vibrations of water molecules or hydroxy and NH groups involved in hydrogen bonding, indicating the gradual dehydration of LaTCM. Moreover, the formation of dehydrated lanthanide tricyanomelaminates is consistent with the behavior of other rare-earth carbon nitrides, such as lanthanide dicyanamides, which are also transformed from hydrated to non-hydrated forms at around 150 °C.[46] Nevertheless, *complete* dehydration of the tricyanomelaminates in the present case is considered rather unlikely, as evidenced by the formation of lanthanide oxides above 700 °C (see Figure S9 in the Supporting Information).

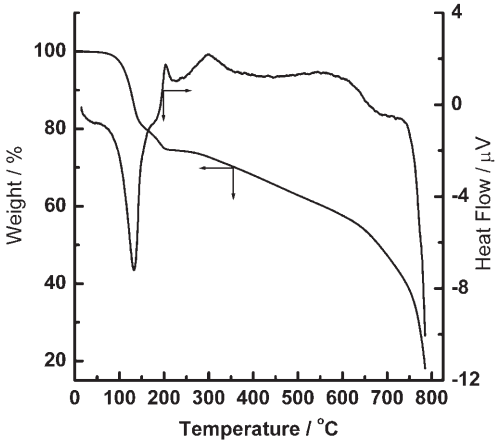


Figure 14. TG–DTA curve of $[NH_4]La[HC_6N_9]_2[H_2O]_7{\cdot}H_2O$ recorded under an argon atmosphere at a heating rate of 10 °C $min^{-1}$.

The second weight loss of 4 % at 200 °C corresponds to partial decomposition of the compounds, and the huge weight loss of 45 % over a wide temperature range between 250 and 800 °C corresponds to gradual decomposition of the tricyanomelaminate moieties followed by the loss of small organic molecules. These events are also indicated by the DTA curve through exothermic peaks at 200, 300, and 560 °C. Above 200 °C, exothermic decomposition occurred, which was followed by amorphization of the samples. This was also evident from vibrational studies, in which the band characteristics of both the triazine core and the cyanamide moieties were seen to change conspicuously after annealing the sample at 200 °C. The sharp signal at around 800 $cm^{-1}$ corresponding to the ring vibration of the tricyanomelaminate moiety remained unchanged, indicating that the triazine core remains intact during heat treatment. However, the characteristic ring "breathing" band appearing at 786 $cm^{-1}$ for the starting monoprotonated tricyanomelaminate is shifted to 800 $cm^{-1}$, thus corroborating the deprotonation of the triazine rings.[52] Moreover, broadening of the band in the region 1300–1600 $cm^{-1}$ and weakening of the signal at 2200 $cm^{-1}$ are indicative of a rearrangement of the tricyanomelaminate moieties through polymerization followed by amorphization of the compounds (see Figure S10 in the Supporting Information). Upon heating above 700 °C, complete decomposition of $[NH_4]La[HC_6N_9]_2[H_2O]_7{\cdot}H_2O$ was observed. Further studies on the pyrolysis of LnTCM are presently underway.

## Discussion

The crystal structures of lanthanide tricyanomelaminates ($[NH_4]Ln[HC_6N_9]_2[H_2O]_7{\cdot}H_2O$) have been solved by a complementary approach based on solid-state MAS NMR and single-crystal X-ray diffraction analysis. Solid-state MAS NMR spectra provide supplementary information concerning the location of hydrogen atoms to the crystal structures of lanthanide tricyanomelaminates. $[NH_4]Ln[HC_6N_9]_2[H_2O]_7{\cdot}H_2O$ was formed as expected from the starting material $[NH_4]_2[HC_6N_9]$ according to Equation (2).

$$\begin{aligned} LnCl_3 \cdot x\,H_2O \;+\; 2\,[NH_4]_2[HC_6N_9] \\ \rightarrow\; [NH_4]Ln[HC_6N_9]_2[H_2O]_7 \cdot H_2O \\ +\; 3\,NH_4Cl \;+\; (x-8)\,H_2O \end{aligned} \qquad (2)$$

A key question concerning the structure of LnTCM is how charge balance is achieved. The deficit of positive

  

charge may be compensated either by protonation of the tricyanomelaminate ion or by ammonium ions, or a mixture of both. Infrared spectra have confirmed the existence of protonated tricyanomelaminate moieties, while solid-state $^{1}H$ MAS NMR spectra gave an initial indication of the presence of an ammonium ion, water molecules, and an N–H group. $^{15}N\{^{1}H\}$ CP NMR spectra have unambiguously confirmed the existence of protonated tricyanomelaminate moieties. In fact, NMR clearly resolves two pairs of strong N–H···N bonds, which correspond to the hydrogen atoms linking the two tricyanomelaminate units. The presence of $[NH_4]^+$ as well as two crystallographically independent monoprotonated tricyanomelaminate ions has been further confirmed by means of $^{15}N$ CP and CPPI experiments. Therefore, it can be concluded that charge balance is achieved by ammonium and monoprotonated tricyanomelaminate ions, where $Ln^{3+}$ and $[NH_4]^+$ cations function as charge-compensating cations for two monoprotonated $[HC_6N_9]^{2-}$ ions.

Using 2D experiments and advanced CP techniques, we have assigned the peaks observed in the $^{1}H$, $^{15}N$, and $^{13}C$ MAS NMR spectra of LaTCM. These assignments may prove helpful in further systematic studies of graphitic carbon nitrides. The thermal stability of LaTCM observed by means of thermal analysis mirrors the proton mobility inferred from temperature-dependent $^{1}H$ MAS NMR spectra, although the latter indicates that significant hydrogen motion on the NMR time scale sets in at around 50 °C, which is below the onset temperature observed in DTA/TG thermograms.

An initial photoluminescence study on $[NH_4]Ln[HC_6N_9]_2[H_2O]_7\cdot H_2O$ (Ln = Eu, Tb) has revealed orange-red and green luminescence for the europium and terbium tricyanomelaminates, respectively. However, their quantum efficiencies proved to be low compared with those of commercial phosphors. It is well known that the non-radiative effect of the OH oscillators of $H_2O$ molecules influences the luminescence features of trivalent lanthanides. Therefore, the low quantum efficiencies of the LnTCM compounds can be ascribed to non-radiative losses due to multiphonon emission involving the water molecules. In addition, significant concentration quenching might be expected due to energy transfer between two adjacent $Tb^{3+}$ or $Eu^{3+}$ ions in TbTCM or EuTCM, respectively. However, the Eu···Eu or Tb···Tb distances within a layer are about 13 Å and those between two layers are about 7 Å, which rules out the possibility of energy migration through exchange interaction (critical distance ($R_c$) = 5 Å) resulting in strong concentration quenching.[62] Only weak multipolar interactions can occur between two $Tb^{3+}$ or $Eu^{3+}$ ions in $[NH_4]Tb[HC_6N_9]_2[H_2O]_7\cdot H_2O$ and $[NH_4]Eu[HC_6N_9]_2[H_2O]_7\cdot H_2O$, respectively. On the other hand, at higher concentrations of the activators, there is also the possibility of cross-relaxation, whereby the higher energy level emissions of $Tb^{3+}$ or $Eu^{3+}$ may be quenched. However, higher quantum efficiencies can be expected for non-hydrated rare-earth tricyanomelaminates and so further studies are in progress aimed at elucidating the crystal structure of these and thereby permitting study of the luminescence properties of non-hydrated phases of lanthanide tricyanomelaminates. Moreover, the isostructural nature of all nine rare-earth tricyanomelaminates (LnTCM; Ln = La, Ce, Pr, Nd, Sm, Eu, Gd, Tb, Dy) also motivates us to explore the photoluminescence that might arise upon doping the isostructural gadolinium or lanthanum tricyanomelaminates ($[NH_4]Ln[HC_6N_9]_2[H_2O]_7\cdot H_2O$; Ln = La, Gd) with $Eu^{3+}$ or $Tb^{3+}$, which would be expected to reduce the concentration quenching by cross-relaxation.

## Conclusion

A series of new rare-earth tricyanomelaminates ($[NH_4]Ln[HC_6N_9]_2[H_2O]_7\cdot H_2O$; Ln = La, Ce, Pr, Nd, Sm, Eu, Gd, Tb, Dy) has been synthesized. Solid-state MAS NMR studies, in conjunction with single-crystal X-ray diffraction analysis, have been instrumental in elucidating the structural network in these compounds, in which the tricyanomelaminate moieties are stacked through hydrogen bonding. This arrangement leads to compounds that are stable even at elevated temperatures. Initial observations of the photoluminescence of europium and terbium tricyanomelaminates, as well as the isostructural nature of all of the nine rare-earth tricyanomelaminates studied, suggest that materials such as lanthanum tricyanomelaminate or gadolinium tricyanomelaminate may represent important host matrices, doping of which with the other rare-earth ions may result in promising phosphors for application in display devices.

## Experimental Section

**Synthesis**: Rare-earth ammonium tricyanomelaminates were prepared by aqueous ion-exchange reactions between the respective lanthanide chlorides ($LnCl_3\cdot x H_2O$) and ammonium tricyanomelaminate ($[NH_4]_2[HC_6N_9]$). In a typical procedure, a column containing 5 mL of strongly acidic ion-exchange resin (Ionenaustauscher I, $H^+$-Form, Art. 4765, Merck) with an ion-exchange capacity of $1.7\times10^{-3}$ mol mL$^{-1}$ was completely filled with a 0.02 M solution of $LnCl_3\cdot xH_2O$ (Ln = La, Ce, Pr, Nd, Sm, Eu, Gd, Tb, or Dy) (Alfa Aesar). Complete loading with $Ln^{3+}$ was indicated by a change in the pH from acidic to neutral, that is, the pH of $LnCl_3\cdot x H_2O$. Once the column was fully loaded, the exchange resin was thoroughly washed with deionized water and complete removal of the excess chloride was verified in that the eluate no longer gave a precipitate with $AgNO_3$. Subsequently, a solution of ammonium tricyanomelaminate (150 mg/20 mL $H_2O$) was applied to the column and the eluate was concentrated to dryness at room temperature. The product obtained was the respective lanthanide tricyanomelaminate ($[NH_4]Ln[HC_6N_9]_2[H_2O]_7\cdot H_2O$; Ln = La, Ce, Pr, Nd, Sm, Eu, Gd, Tb, Dy), which proved isostructural throughout the series, in the form of tiny rod-shaped crystals, irrespective of the concentration of the ammonium tricyanomelaminate starting material.

Ammonium tricyanomelaminate was synthesized by aqueous ion-exchange between ammonium chloride and sodium tricyanomelaminate, the procedure for which has been described in detail by Lotsch et al.[10] Sodium tricyanomelaminate was obtained by annealing sodium dicyanamide ($Na[C_2N_3]$; Fluka, >96 %) at ≈500 °C in a sealed quartz ampoule under argon atmosphere.[36]

**X-ray diffraction**: X-ray diffraction data were collected from a single crystal of LaTCM at room temperature on a STOE IPDS single-crystal

  

diffractometer using graphite-monochromated $Mo_{K\alpha}$ radiation ($\lambda = 0.71073$ Å). A semiempirical absorption correction based on the intensities of equivalent reflections was applied. The crystal structure was solved by direct methods using the software package SHELXS-97[67] and refined by the full-matrix least-squares method as implemented in SHELXL-97[68] with anisotropic displacement parameters for all non-hydrogen atoms.

For X-ray diffraction investigation of the rare-earth tricyanomelaminates LnTCM (Ln = Ce, Pr, Nd, Sm, Eu, Gd, Tb, Dy), powdered samples were enclosed in glass capillaries of diameter 0.3 mm. The measurements were carried out in Debye–Scherrer geometry on a STOE Stadi P powder diffractometer using Ge(111)-monochromated $Mo_{K\alpha1}$ radiation ($\lambda = 0.7093$ Å). The X-ray diffractometry study indicated that the diffraction pattern of LnTCM (Ln = Ce, Pr, Nd, Sm, Eu, Gd, Tb, Dy) could be indexed with similar lattice constants and the same space group as in the case of LaTCM (Figure 1). Hence, Rietveld refinements were performed with the program GSAS[59] using the atomic coordinates of LaTCM as the starting values. To describe the profile of the X-ray reflections, a pseudo-Voigt function was used.[60,61]

CCDC-620795 (LaTCM), CCDC-620786 (CeTCM), CCDC-620806 (PrTCM), CCDC-620805 (NdTCM), CCDC-621093 (SmTCM), CCDC-620803 (EuTCM), CCDC-620804 (GdTCM), CCDC-620807 (TbTCM), and CCDC-620802 (DyTCM) contain the supplementary crystallographic data for this paper. These data can be obtained free of charge from the Cambridge Crystallographic Data Centre via www.ccdc.cam.ac.uk/data_request/cif.

High-temperature in situ X-ray diffractometry was performed on a STOE Stadi P powder diffractometer (Ge(111)-monochromated $Mo_{K\alpha1}$ radiation, $\lambda = 0.7093$ Å) with an integrated furnace, using unsealed quartz capillaries (0.5 mm) as sample containers. The data collection was restricted to a $2\theta$ range of approximately 3–20° with an average scan collection time of 34 min. The samples were heated from room temperature to around 800 °C in increments of 25 °C.

**Solid-state NMR spectroscopy**: $^1$H, $^{13}$C, and $^{15}$N CP MAS solid-state NMR spectra of LaTCM were recorded at ambient temperature on a DSX Avance NMR spectrometer (Bruker) in a magnetic field of 11.74 T. The samples were contained in 4 mm or 2.5 mm $ZrO_2$ rotors, which were mounted in commercial MAS probes and examined in double-resonance mode. The $^1$H and $^{13}$C signals were referenced to tetramethylsilane (TMS), while the $^{15}$N signals were referenced to nitromethane. In the 1D CP experiments, a contact time of 4 ms, a recycle delay of 1 s, and a spinning frequency of 10 kHz were employed for both the $^{13}$C and $^{15}$N MAS NMR measurements. During all of the CP experiments, we used CW $^1$H decoupling during the FID, with a decoupling field strength of approximately 80 kHz. The nutation frequency of hard $^1$H pulses typically applied during CP, BABA,[56] and DEPTH[55] experiments was 80 kHz.

A ramped cross-polarization[69] sequence was employed to excite the $^{15}$N nuclei via proton bath, whereby the power of the $^1$H radiation was varied linearly by about 50 %. A CPPI (cross-polarization combined with polarization inversion) experiment was performed to probe the number of hydrogen atoms directly attached to the nitrogen atoms present in LaTCM. For this, an inversion time of 160 μs and a contact time of 10 ms were used. The recycle delay was set at 1 s, as derived from $^1$H T1 measurements, and the spinning frequency was 6 kHz.

In the variable-temperature $^1$H NMR experiments, the temperature was externally calibrated using the $^{207}$Pb resonance of crystalline $Pb(NO_3)_2$.[70,71] The chemical shift scale is referenced to $Pb(CH_3)_4$, determined from TMS using the IUPAC conversion factors.[72] We used the linear relationship between temperature and chemical shift given in Equation (3), which was compiled from literature data:

$$\delta_{iso}(^{207}Pb) = 0.760\ ppm/KT + 3714\ ppm \quad (3)$$

$^1$H MAS NMR spectra were recorded using a DEPTH pulse sequence[55] with four 180° pulses to ensure proton background suppression. The double-quantum filtered 2D correlation spectrum was acquired with a zero-quantum filtered BABA pulse sequence[56] at a sample spinning frequency of 30 kHz, using two rotor periods for double-quantum excitation and reconversion. The time increment of the indirect dimension was equal to a rotor period.

**Vibrational spectroscopy**: FTIR measurements were carried out on a Bruker IFS 66v/S spectrometer. Spectra were recorded under ambient conditions over the range 400 to 4000 $cm^{-1}$ after dispersing the samples in anhydrous KBr pellets (1 mg sample, 500 mg KBr).

**Thermal analysis**: Thermoanalytical measurements were performed on a simultaneous thermogravimetry/differential thermal analyzer (Setaram thermoanalyzer TGA 92–2400) in the temperature range 25 to 800 °C (heating rate 10 °C $min^{-1}$) under an argon atmosphere. The thermal behavior of the LnTCM compounds was studied under isothermal conditions on a preparative scale by annealing the samples under argon atmosphere in sealed glass or quartz ampoules by heating them to various temperatures between 100 and 800 °C at a heating rate of 1 °C $min^{-1}$. The resulting products were characterized by X-ray powder diffraction and IR spectroscopy.

**Photoluminescence studies**: Diffuse reflectance spectra of the powder samples were recorded between 200 and 700 nm with a Varian Cary 500 spectrophotometer. The excitation (PLE) and emission (PL) spectra were obtained at room temperature using an FL900 spectrofluorimeter (Edinburgh Instruments) with an Xe lamp as a light source, fitted with a Hamamatsu photomultiplier. The presented excitation and emission spectra have been corrected for the sensitivity of the FL900 spectrofluorimeter and the characteristics of the excitation lamp.

The quantum efficiencies (QE) of the novel phosphors were determined by comparison with those of standard phosphors, the values of which have been reported previously.[66] The standard phosphors used were lumogen red, a perylene dye (BASF, QE = 42.3 % for 365 nm excitation), for $Eu^{3+}$ samples, and laboratory phosphor $SrSi_2N_2O_2$:Eu (Philips Lighting Components, QE = 81.3 % for 365 nm excitation), for $Tb^{3+}$ samples.

For the calculation of CIE (Commission Internationale d'Eclairage) color coordinates ($x$, $y$), the emission spectra were weighted by 10° standard observer CIE color matching functions. After summarizing, the obtained tristimulus values were normalized to obtain CIE 1933 color coordinates.

## Acknowledgements

The authors thank J. Kechele and A. Sattler for conducting the TG/DTA measurements, T. Miller for performing the temperature-dependent powder X-ray diffraction studies, and C. Minke for the solid-state MAS NMR measurements (all at the Department of Chemistry and Biochemistry, Ludwig-Maximilians-Universität München). Financial support from the Deutsche Forschungsgemeinschaft (DFG) (Schwerpunktprogramm "Lanthanoidspezifische Funktionalitäten in Molekül und Material", project SCHN 377/10–2), the Emmy-Noether Programm (DFG, SCHM 1570–2/1), and the Fonds der Chemischen Industrie (FCI) is gratefully acknowledged.

[1] M. L. Cohen, *Phys. Rev. B* **1985**, *32*, 7988–7991.
[2] A. Y. Liu, M. L. Cohen, *Science* **1989**, *245*, 841–842.
[3] A. Y. Liu, M. L. Cohen, *Phys. Rev. B* **1990**, *41*, 10727–10734.
[4] M. L. Cohen, *Science* **1993**, *261*, 307–308.
[5] C. Niu, Y. Z. Lu, C. M. Lieber, *Science* **1993**, *261*, 334–337.
[6] D. M. Teter, R. J. Hemley, *Science* **1996**, *271*, 53–55.
[7] B. Jürgens, E. Irran, J. Senker, P. Kroll, H. Müller, W. Schnick, *J. Am. Chem. Soc.* **2003**, *125*, 10288–10300.
[8] E. Kroke, M. Schwarz, *Coord. Chem. Rev.* **2004**, *248*, 493–532.
[9] B. V. Lotsch, W. Schnick, *Chem. Mater.* **2005**, *17*, 3976–3982.
[10] B. V. Lotsch, W. Schnick, *Chem. Mater.* **2006**, *18*, 1891–1900.
[11] J. von Liebig, *Ann. Pharm.* **1834**, *10*, 1–47.
[12] I. Alves, G. Demazeau, B. Tanguy, F. Weill, *Solid State Commun.* **1999**, *109*, 697–701.
[13] Z. Zhang, K. Leinenweber, M. Bauer, L. A. J. Garvie, P. F. McMillan, G. H. Wolf, *J. Am. Chem. Soc.* **2001**, *123*, 7788–7796.

  

[14] G. H. Wolf, M. Bauer, K. Leinenweber, L. A. J. Garvie, Z. Zhang, NATO Sci. Ser., II: Mathematics, Physics, and Chemistry **2001**, 48 (Frontiers of High-Pressure Research II: Application of High Pressure to Low-Dimensional Novel Electronic Materials), p. 29.
[15] M. Kawaguchi, K. Nozaki, *Chem. Mater.* **1995**, *7*, 257–264.
[16] V. N. Khabashesku, J. L. Zimmermann, J. L. Margrave, *Chem. Mater.* **2000**, *12*, 3264–3270.
[17] E. G. Gillan, *Chem. Mater.* **2000**, *12*, 3906–3912.
[18] M. Mattesini, S. F. Matar, J. Etourneau, *J. Mater. Chem.* **2000**, *10*, 709–713.
[19] X. Liu, P. Kroll, R. Dronskowski, *Z. Anorg. Allg. Chem.* **2001**, *627*, 1682–1686.
[20] W. Liao, C. Hu, R. Dronskowski, *Acta Crystallogr. Sect. E* **2003**, *59*, m1124–m1126.
[21] S. R. Batten, K. S. Murray, *Coord. Chem. Rev.* **2003**, *246*, 103–130.
[22] D. R. Miller, D. C. Swenson, E. G. Gillan, *J. Am. Chem. Soc.* **2004**, *126*, 5372–5373.
[23] E. Horvath-Bordon, E. Kroke, I. Svoboda, H. Fueß, R. Riedel, N. Sharma, A. K. Cheetam, *Dalton Trans.* **2004**, *22*, 3900–3908.
[24] E. Horvath-Bordon, E. Kroke, I. Svoboda, H. Fueß, R. Riedel, *New J. Chem.* **2005**, *29*, 693–699.
[25] X. Liu, M. Krott, P. Müller, C. Hu, H. Lueken, R. Dronskowski, *Inorg. Chem.* **2005**, *44*, 3001–3003.
[26] P. Starynowicz, *Acta Crystallogr. Sect. C* **1991**, *47*, 2198–2199.
[27] U. Berger, W. Schnick, *J. Alloys Compd.* **1994**, *206*, 179–182.
[28] M. Kurmoo, C. J. Kepert, *New J. Chem.* **1998**, *22*, 1515–1524.
[29] S. R. Batten, P. Jensen, B. Moubaraki, K. S. Murray, R. Robson, *Chem. Commun.* **1998**, 439–440.
[30] J. L. Manson, C. R. Kmety, Q.-Z. Huang, J. W. Lynn, G. M. Bendele, S. Pagola, P. W. Stephens, L. M. Liable-Sands, A. L. Rheingold, A. J. Epstein, J. S. Miller, *Chem. Mater.* **1998**, *10*, 2552–2560.
[31] S. R. Batten, P. Jensen, C. J. Kepert, M. Kurmoo, B. Moubaraki, K. S. Murray, D. J. Price, *J. Chem. Soc. Dalton Trans.* **1999**, 2987–2997.
[32] J. L. Manson, C. R. Kmety, A. J. Epstein, J. S. Miller, *Inorg. Chem.* **1999**, *38*, 2552–2553.
[33] P. Jensen, D. J. Price, S. R. Batten, B. Moubaraki, K. S. Murray, *Chem. Eur. J.* **2000**, *6*, 3186–3195.
[34] M. Becker, J. Nuss, M. Jansen, *Z. Anorg. Allg. Chem.* **2000**, *626*, 2505–2508.
[35] B. Jürgens, E. Irran, J. Schneider, W. Schnick, *Inorg. Chem.* **2000**, *39*, 665–670.
[36] M. Becker, M. Jansen, *Solid State Sci.* **2000**, *2*, 711–717.
[37] E. Irran, B. Jürgens, W. Schnick, *Chem. Eur. J.* **2001**, *7*, 5372–5381.
[38] B. Jürgens, E. Irran, W. Schnick, *J. Solid State Chem.* **2001**, *157*, 241–249.
[39] J. L. Manson, C. R. Kmety, F. Palacio, A. J. Epstein, J. S. Miller, *Chem. Mater.* **2001**, *13*, 1068–1073.
[40] B. Jürgens, E. Irran, H. A. Höppe, W. Schnick, *Z. Anorg. Allg. Chem.* **2004**, *630*, 219–223.
[41] X. Liu, P. Müller, R. Dronskowski, *Z. Anorg. Allg. Chem.* **2005**, *631*, 1071–1074.
[42] E. Irran, B. Jürgens, S. Schmid, W. Schnick, *Z. Anorg. Allg. Chem.* **2005**, *631*, 1512–1515.
[43] O. Reckeweg, F. J. DiSalvo, *Z. Anorg. Allg. Chem.* **2003**, *629*, 177–179.
[44] R. Srinivasan, M. Ströbele, H.-J. Meyer, *Inorg. Chem.* **2003**, *42*, 3406–3411.
[45] B. Jürgens, E. Irran, W. Schnick, *J. Solid State Chem.* **2005**, *178*, 72–78.
[46] A. Nag, W. Schnick, *Z. Anorg. Allg. Chem.* **2006**, *632*, 609–614.
[47] B. Jürgens, H. A. Höppe, W. Schnick, *Solid State Sci.* **2002**, *4*, 821–825.
[48] B. Jürgens, W. Milius, P. Morys, W. Schnick, *Z. Anorg. Allg. Chem.* **1998**, *624*, 91–97.
[49] E. Irran, B. Jürgens, W. Schnick, *Solid State Sci.* **2002**, *4*, 1305–1311.
[50] B. F. Abrahams, S. J. Egan, B. F. Hoskins, R. Robson, *Chem. Commun.* **1996**, 1099–1100.
[51] B. F. Abrahams, S. J. Egan, B. F. Hoskins, R. Robson, *Acta Crystallogr. C* **1996**, *52*, 2427–2429.
[52] B. Jürgens, H. A. Höppe, W. Schnick, *Z. Anorg. Allg. Chem.* **2004**, *630*, 35–40.
[53] R. Mueller-Mach, G. Mueller, M. R. Krames, H. A. Höppe, F. Stadler, W. Schnick, T. Juestel, P. Schmidt, *Phys. Status Solidi A* **2005**, *202*, 1727–1732.
[54] A. Nag, P. J. Schmidt, W. Schnick, *Chem. Mater.* in press.
[55] D. G. Cory, W. M. Ritchey, *J. Magn. Reson.* **1988**, *80*, 128–132.
[56] M. Feike, D. E. Demco, R. Graf, J. Gottwald, S. Hafner, H. W. Spiess, *J. Magn. Reson. A122*, 214–221.
[57] E. Kroke, M. Schwarz, E. Horath-Bordon, P. Kroll, B. Noll, A. D. Norman, *New J. Chem.* **2002**, *26*, 508–512.
[58] C. Gervais, F. Babonneau, J. Maquet, C. Bonhomme, D. Massiot, E. Framery, M. Vaultier, *Magn. Reson. Chem.* **1998**, *36*, 407–414.
[59] A. C. Larson, R. B. von Dreele, *General structure analysis system*, Report LAUR 86–748, Los Alamos National Laboratory, Los Alamos, NM, **1990**.
[60] P. Thompson, D. E. Cox, A. P. Hastings, *J. Appl. Crystallogr.* **1987**, *20*, 79–83.
[61] L. W. Finger, D. E. Cox, A. P. Jephcoat, *J. Appl. Crystallogr.* **1994**, *27*, 892–900.
[62] G. Blasse, B. C. Grabmeier, *Luminescent Materials*, Springer, Berlin, **1998**.
[63] C. Görller-Walrand, K. Binnemans, *Handbook on the Physics and Chemistry of Rare-Earths, Vol. 25* (Eds.: K. A. Gschneider, Jr., L. Eyring), North Holland, Amsterdam, **1998,** Chapter 167.
[64] B. R. Judd, *Phys. Rev.* **1962**, *127*, 750–761.
[65] G. S. Ofelt, *J. Chem. Phys.* **1962**, *37*, 511–520.
[66] T. Jüstel, J. C. Krupa, D. U. Wiechert, *J. Lumin.* **2001**, *32*, 179–189.
[67] G. M. Sheldrick, SHELXS-97, Program for solution of crystal structures, University of Göttingen, Germany, **1997**.
[68] G. M. Sheldrick, SHELXL-97, Program for refinement of crystal structures, University of Göttingen, Germany, **1997**.
[69] G. Metz, X. Wu, S. O. Smith, *J. Magn. Reson.* **1994**, *A110*, 219–227.
[70] G. Neue, C. Dybowski, *Solid State Nucl. Magn. Reson.* **1997**, *7*, 333–336.
[71] A. Bielecki, D. P. Burum, *J. Magn. Reson.* **1995**, *A116*, 215–220.
[72] R. K. Harris, E. D. Becker, *J. Magn. Reson.* **2002**, *156*, 323–326.

Received: September 20, 2006
Published online: February 16, 2007

  